

1170, Dec. 1974.

[17] A. S. Clorfeine, R. J. Ikola, and L. S. Napoli, "A theory for the high-efficiency mode of oscillation in avalanche diodes," *RCA Rev.*, vol. 30, pp. 397-421, Sept. 1969.

[18] T. E. Seidel, R. E. Davis, and D. E. Iglesias, "Double-drift region ion-implanted millimeter-wave IMPATT diodes," *Proc. IEEE (Special Issue on Microwave Semiconductors)*, vol. 59, pp. 1222-1228, Aug. 1971.

[19] R. S. Ying, "X-band silicon double-drift IMPATT diodes using multiple epitaxy," *Proc. IEEE (Lett.)*, vol. 60, pp. 1104-1105, Sept. 1972.

[20] R. W. Bierig, R. Bera, and M. R. Harris, "Complementary TRAPATT mode oscillations," in *1972 ISSCC Dig.* (Philadelphia, Pa.), pp. 200-201, Feb. 1972.

[21] G. I. Haddad, C. M. Lee, and W. E. Schroeder, "An approximate comparison between  $n^+p-p^+$  and  $p^+n-n^+$  silicon TRAPATT diodes," *IEEE Trans. Microwave Theory Tech. (Short Papers)*, vol. MTT-21, pp. 501-502, July 1973.

[22] J. E. Carroll and R. H. Crede, "A computer simulation of TRAPATT circuits," *Int. J. Electron.*, vol. 32, pp. 273-296, 1972.

[23] B. Culshaw, "Time-domain model of the device/circuit characteristics of a trapped-plasma avalanche-diode oscillator," *Electron. Lett.*, vol. 7, pp. 339-340, June 1971.

## Satellite Altimetry Applications

JOSEPH T. McGOOGAN

**Abstract**—This paper provides a brief background of precision satellite altimetry. A description of satellite altimetry concepts and instrumentation is presented. The parameters measured, supporting data, and techniques, as well as physical limitations, are discussed. In addition, results are shown and a variety of applications is emphasized.

### INTRODUCTION AND BACKGROUND

**SATELLITE** altimetry is primarily devoted to active sensing of the ocean-surface topography which is then utilized for geodetic and oceanographic studies.

The long-term objectives of satellite altimetry were stated in the 1969 Williamstown study on Solid Earth and Ocean Physics [1] and the 1972 Earth and Ocean Physics Applications Program (EOPAP) report. These studies call for development of a 10-cm-accurate synoptic satellite altimeter with at least  $1^\circ$  (100-km) spatial resolution.

### SATELLITE ALTIMETRY CONCEPT

The basic idea behind altimetry is to utilize the highly stable platform provided by a satellite as a moving reference system from which vertical measurements to the ocean surface are made (see Fig. 1). The altimeter measures to the instantaneous electromagnetic mean sea level (IEMSL) averaged over the spatial footprint of the instrument.

The IEMSL can be related to the mean sea level (MSL) if the relationship between the radar mean return point, and mean sea height is known. However, MSL often varies because of currents, tides, storm surges, etc. Most

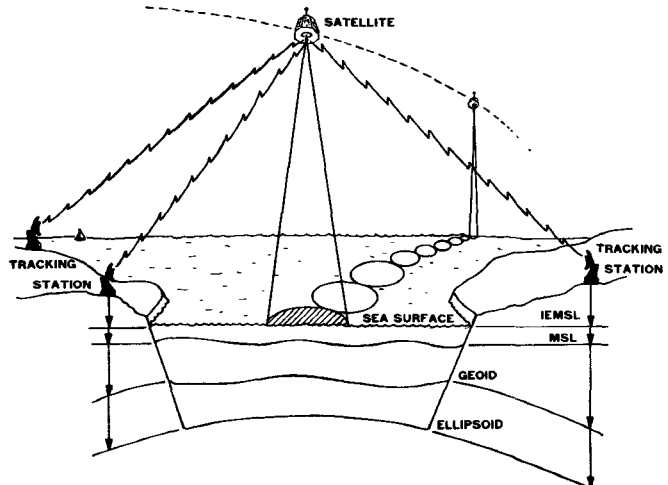


Fig. 1. Satellite altimetry geometry.

of these dynamic ocean effects can be removed if observations are taken over an extended time. The residual steady-state ocean surface topography is directly related to the shape of the geoid.

### INSTRUMENTATION

The Skylab radar altimeter was the first in a series of satellite altimeters that are planned to progressively achieve the EOPAP goals. This altimeter was designed primarily for obtaining the radar technology for designing improved altimeters. Currently, the GEOS-C altimeter launched April 9, 1975, will be the first globally applied system. In 1978 the SEASAT-A altimeter will be a part of an ocean-dedicated satellite instrumentation system and will be the first attempt to achieve 10-cm resolution [2]. A comparison of these satellite systems is presented in Table I.

Manuscript received April 18, 1975; revised July 21, 1975.

The author is with the Wallops Flight Center, National Aeronautics and Space Administration, Wallops Island, Va. 23337.

TABLE I

	SKYLAB	GEOS-C (Intensive Mode)	SEASAT-A
Mean Altitude	435 km	840 km	800 km
Antenna Beamwidth	1.5°	2.6°	1.5°
Frequency	13.9 GHz	13.9 GHz	13.9 GHz
Peak Power	2 kw	2 kw	2 kw
Pulsewidth	100 n sec	12.5 n sec	3 n sec
Single Pulse SNR	21 db	12 db	20 db
Footprint Size	8 km	3.6 km	1.6 km
Altitude Precision	< 1 m rms	< 0.6 m rms	10 cm rms

Existing altimeters are basically conventional monostatic tracking radars which track in range only. The instrumentation utilized on Skylab and planned for GEOS-C and SEASAT-A makes three basic measurements: altitude (range), waveforms, and automatic gain control (AGC) [3], [4].

The time interval from transmit time to the half-power point of the leading edge of the return is proportional to altitude. These transit times are measured with a closed-loop tracking system with bandwidths of a few hertz to follow the dynamics of the ocean surface. Local vertical-height measurements are made via a pulse-length-limited geometry. This is achieved by using a small antenna such that the beamwidth is larger than the pulse-length-limited footprint or the combined pulse- and sea-state-limited footprint. The effect of sea state on the footprint is illustrated in Fig. 2.

A simple (first-order only) model of the return waveforms can be based on physical-optics scattering theory [5]. It can be seen in Fig. 3 that the illuminated surface area determines the reflected radar power as the pulse impinges on the earth's spherical surface. This back-scattered power (on the average) increases until the whole pulse has reached the surface. From this time on, the mean power will tend to have a constant value as other annular surface areas are illuminated. This causes the return pulse to have a flat plateau region that extends in time until the limitation of the antenna beamwidth cuts off the signal.

From this model it appears that the return-pulse rise time is set by the transmitted-pulse time duration.

However, as shown in Fig. 2, the pulsewidth or sea state (depending on which represents the larger time spread to the altimeter) determines the footprint size. This footprint acts as a spatial filter that has to be considered in detecting surface features (see Fig. 4). Its minimum radius is calculated as follows:  $r = (hcT)^{1/2}$  where  $h$  = satellite height,  $c$  = speed of light,  $T$  = pulsewidth.

The satellite waveform data typically consist of samples at appropriate intervals (consistent with their bandwidth) obtained with high-speed sample-and-hold cir-

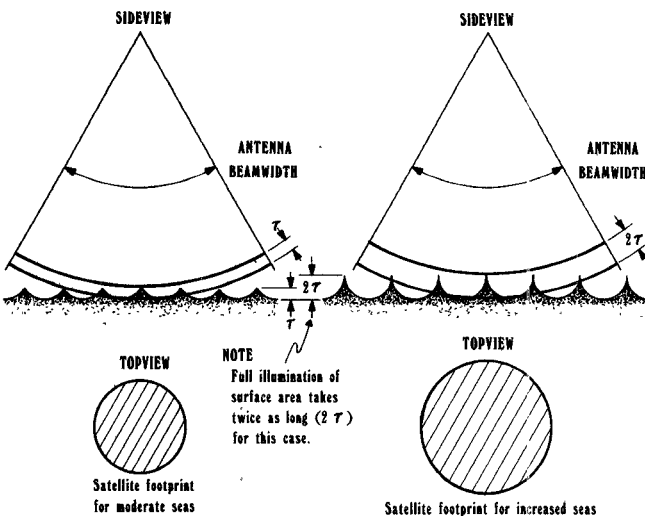


Fig. 2.

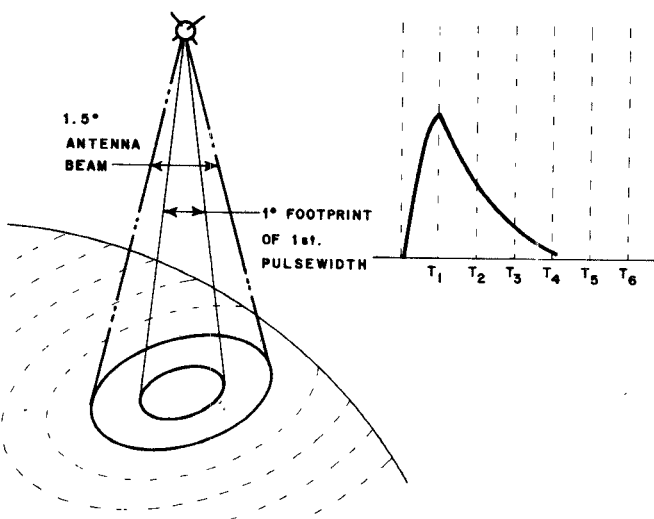


Fig. 3. Case 1: antenna beam pointed directly at nadir.

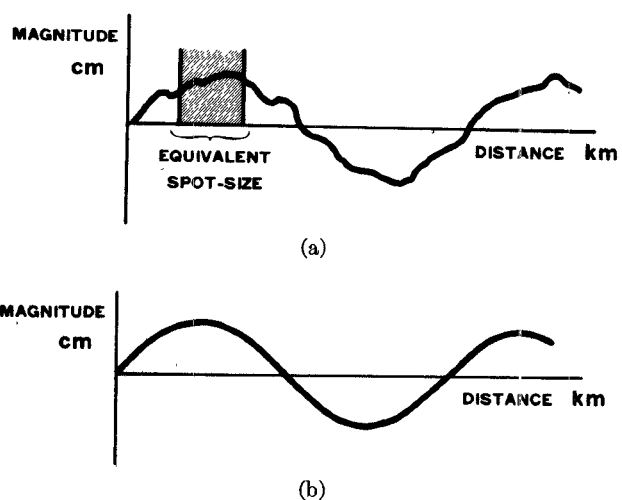


Fig. 4. (a) Possible geodetic signal in relation to radar altimeter footprint. (b) Signal resulting from a "moving-window" average of (a).

ciuity. These sampled data are then utilized on the ground to reconstruct the spacecraft waveforms for further analysis.

The AGC voltage utilized to normalize the mean signal levels for processing is also a source of reflectivity data. Typically, the bandwidth of this circuit is slightly less than the altitude tracker and therefore is not sampled as often.

### TECHNIQUES AND LIMITATIONS

To support satellite altimetry some special new techniques have had to be developed which include the orbit determination, instrument calibration, determination of satellite pointing, and data corrections. In addition, while the instrumentation techniques required have not been entirely new, they have had to be applied to altimetry and made compatible with a spacecraft environment. Some challenging developments have been made in pulse compression, pulse stretch, maximum likelihood processing, and high-voltage power supplies [2].

These areas of technological development are also the major areas that limit altimetry. For example, the pulsewidth determines the footprint which limits the spacial resolution and the measurement of wave heights. Likewise, the orbit accuracy limits altimetry accuracy for mapping the broad-scale ocean topography (see Table II). However, the absolute orbit error may not be important. It is thought that if a large density of altimeter data can be collected, it can be used to constrain itself [6].

In Table II the Skylab altimeter is used to show the present state of altimeter system accuracy [6]. The uncorrected column shows the quality of the raw data using the Johnson Space Center orbit which was not designed for geodesy. The corrected column shows an improved accuracy with some basic corrections that can easily be made.

### Instrument Errors

The largest instrument errors are biases brought about by changes in operating parameters (pulsewidth, bandwidth, etc.). The magnitude of these errors can easily be detected over the flat sea surface since they appear as sharp height steps. Once the magnitude is known, the

corrections can be applied coincident with the change of operating mode.

In addition, an initial zero set bias for the instrument must be established. Prelaunch system delays can be compiled to provide a first approximation correction for this error. Comparison between the satellite altimeter and independent orbit tracking systems with simultaneous measurements of the sea surface height would provide a more practical measure of the bias. However, it must be remembered that these methods are also subject to bias. Therefore, independent techniques are primarily useful to confirm that the altimeter measurement system is not drifting.

To calibrate the GEOS-C satellite, a calibration area off the east coast of the United States has been established. A detailed geoid map and tide model for this area has been produced. In addition, tide gauges have been installed around this area, and a network of lasers and radars are committed to measure the position of the orbit.

In addition to these external techniques, each altimeter is designed with an internal calibration mode. The transmitter pulse is usually attenuated, delayed, and inserted in the receiver channel so that the tracking system can measure its time position (height). This measurement will provide an automatic means of regularly monitoring the drift of most of the internal circuits of the system.

### Pointing

Pointing errors are determined by the analysis of the trailing edge of the return signal waveforms (see Fig. 5). For nadir pointing, the shape of the trailing edge is determined by the antenna pattern, whereas pointing errors cause amplitude distortions (changes in slope). The smaller the antenna pattern in comparison to the pulsewidth, the more sensitive the system is to pointing errors. Since there is also some detrimental effect of pointing errors on the entire return waveshape, antenna pointing information is valuable for refining the altitude and ocean wave-height determination. However, it should be noted that the trailing edge of the pulse is least sensitive to jitter and therefore is usable for very precise determination of pointing errors.

TABLE II

	SKYLAB	
	Uncorrected	Corrected
1. Instrument Errors		
Systematic	up to 30 meters	< 2 meters
Random	.6 meters (over 1 sec.)	.6 meters
2. Pointing	up to 60 meters	< 5 meters
3. Ocean Surface	Up to .75 meters	< .75 meters
4. Atmospheric		
Tropospheric (dry) {	< 3 meters	< .6 meters using fixed 2.79 m
(wet)		
Ionospheric		
5. Orbit	< 100 meters (JSC)	< 10 meters (WFC)
System Capability for Global Mapping	< ± 100 meters	< ± 10 meters

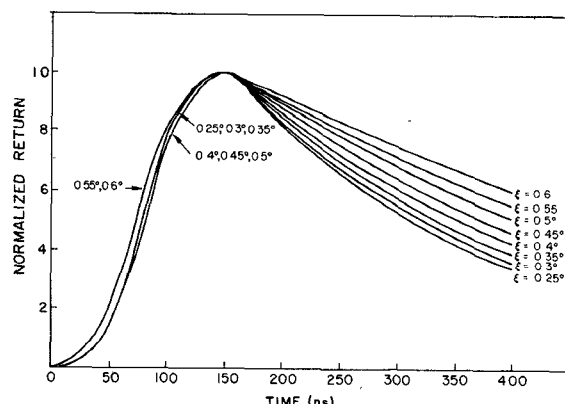


Fig. 5. "Flat sea" return for no jitter,  $h = 235$  nmi.

By optimizing this technique, it should be useful for determining pointing errors up to approximately  $1^\circ$  and yield corrections to height that will correct these errors down to a residual under 10 cm. However, on the Skylab mission, errors larger than  $1^\circ$  occurred commonly, and therefore an alternate technique using the AGC and servo response as an indicator was utilized [6]. This technique was less accurate; hence the residual errors for that satellite are felt to be approximately 5 m.

#### Ocean Surface

Ocean surface effects such as nonuniform reflectivity distributed on the wave heights can also cause a bias. The bias is between the true MSL and the altimeter-measured mean. This bias is small, but models for the error and its correction are not well defined. Therefore, at the present time no corrections are being applied. However, the wave heights can be recovered from the altimeter if at some future time a reflectivity bias versus wave-height calibration curve is available.

Ocean wave-height data are obtained by analyzing the leading edge of the return-signal waveforms [7]. The higher sea states effectively give both earlier and later returns to the altimeter such that the rise time is rounded and resloped as shown in Fig. 6. The narrower the transmitter pulse the sharper the return rise time and the more sensitive the system is to the wave height.

As can be seen from Fig. 6, the slope of the leading edge of the mean return waveforms provides a measure of wave height. Perhaps more importantly, the final waveforms reconstructed on the ground can be thought of as consisting of a convolution of transmitted pulsewidth, attenuation in time due to antenna pattern, range tracker jitter, and distribution of wave heights shown in Fig. 7. Therefore, by either differentiating the leading edge of the returns or comparing them with modeled waveforms, the distribution of wave heights can be obtained.

#### Atmosphere

Without corrections for atmospheric delay, the error would not exceed 3 m [8]. However, it was decided that

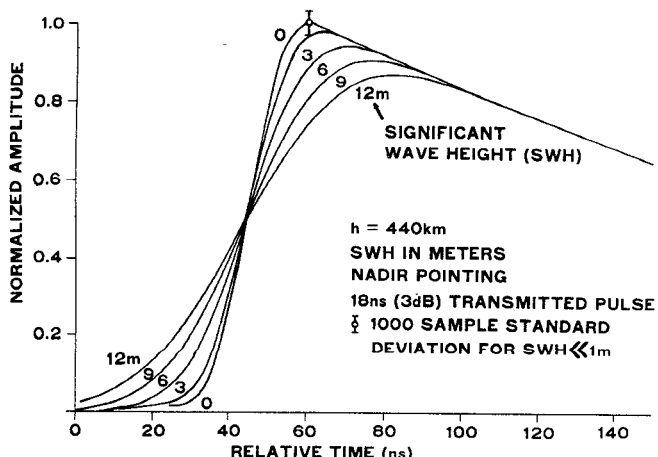


Fig. 6. Typical waveforms showing effect of rms roughness on altimeter signal.

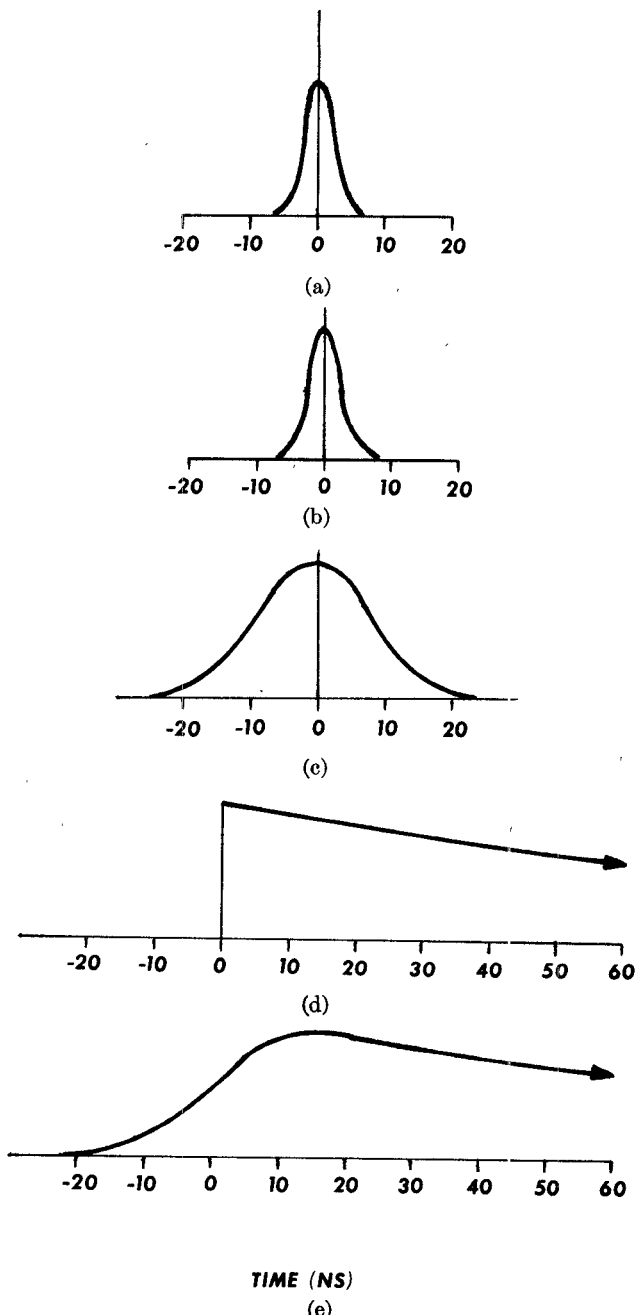


Fig. 7. (a) Range noise distribution. (b) Pulse shape. (c) Surface height distribution. (d) Exponential attenuation in time due to antenna pattern. (e) Composite convolved (a), (b), (c), (d) pulse shape.

a mean correction would be used which left residual errors of approximately 50 cm. As altimeter accuracies increase, first, mean atmospheric conditions for more localized areas will be utilized to refine these residuals down to under 20 cm. Finally, as 10-cm altimetry is approached, it is visualized that global weather data and an on-board microwave radiometer measurement of total moisture will be utilized for further refinements.

#### Orbits

Since radial orbit errors propagate directly into geoid height, and orbit errors are some of the larger errors, these

must be given special attention [6]. For each orbit obtained, a comparison error analysis was performed. The effects of station location errors, gravity model errors, and refraction errors were calculated and propagated into satellite altitude effects. From these studies orbits can be optimized to minimize the altitude errors for each pass or even each subportion of a pass. The major source of uncorrected orbit error in Table II is that the Johnson Space Center gravity model was truncated after five terms.

#### Overall Errors

The overall accuracy shown in the table was confirmed by comparing all the Skylab data to the GEM 6 geoid [9]. In this comparison a histogram of 130 short arcs differenced from the GEM 6 geoid had an rms error of approximately 10 m. This error is felt to be composed primarily of orbit and present geoid uncertainty.

For GEOS-C, the orbit is higher and more tracking stations will be available. In addition, the existing GEM 6 geoid will not have to be used as a standard, for sufficient altimeter data will be available so that an altimeter-measured geoid can be constructed. Therefore, the overall accuracy of GEOS-C should represent a substantial improvement.

### ALTIMETER APPLICATIONS

#### Geoid Determination

Since the water surface of the ocean has the unique property of seeking an equilibrium with the equipotential gravity forces, and since the satellite altimeter provides a direct measurement of the shape of this ocean surface (Fig. 8), the altimeter measurements over ocean surfaces are almost direct geoid measurements [6].

The relationship between geoid height ( $h_g$ ) and satellite altitude measurements is given by

$$h_g = h_s - h_a - \Delta h$$

where

$h_s$  satellite height above a reference spheroid obtained

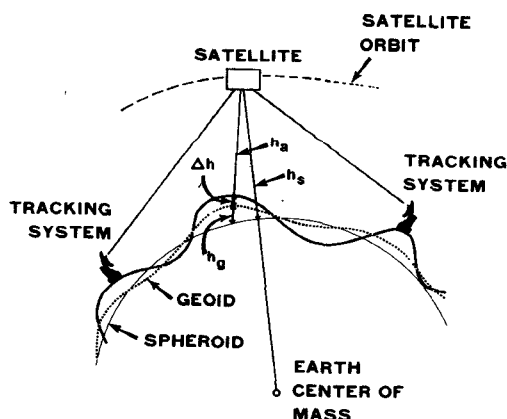


Fig. 8.

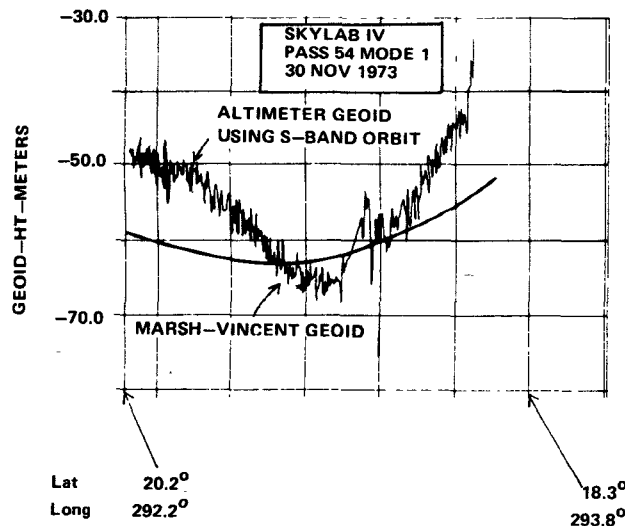


Fig. 9.

from the satellite orbit determined from tracking data;

$h_a$  satellite altitude measured by the altimeter;

$\Delta h$  dynamic ocean effects of tides, winds and currents.

The relationship of these quantities is shown in Fig. 8.

Probably the most significant results of satellite altimetry are in the detection of short-wavelength features such as trenches, seamounts, ridges, and caps. Since the orbit of the satellite acts like a low-pass filter and does not respond to short-wavelength features, the orbit is not a significant error source in mapping the shape of short-wavelength features. Fig. 9 shows a comparison of altimeter data and the Marsh-Vincent (GEM 6) geoid over the Puerto Rico trench area.

#### Correlation with Ocean Floor Topography

During the early phase of the Skylab program, the data recorded in the overwater passes off Charleston, S.C., showed abrupt changes in MSL which were not immediately obvious in existing geoidal data. Fig. 10 illustrates this effect: note the 8-m change which occurs near time 17 h 12 min 22 s, also note the Marsh-Vincent (GEM 6) geoidal contour. The geoidal data available for use were computed using a  $1^\circ \times 1^\circ$  grid [9]. Therefore, to place the altimeter and geoid contours on a comparative basis, the altimeter data were smoothed beyond those required for minimum-mean-square-error considerations, and to a degree which simulates a  $1^\circ \times 1^\circ$  resolution. One can easily see that the unsmoothed altimeter data contain the resolution to detect features that are caused by underwater topography. Therefore, the altimeter can be used to determine when, where, and how to consider local topography in geoid models. In this manner a large quantity of topographic data can be utilized to immediately improve the resolution of the geoid and might later be used to fill in gaps between satellite altimeter geoid measurements. In addition, in areas where the topography is not well known,

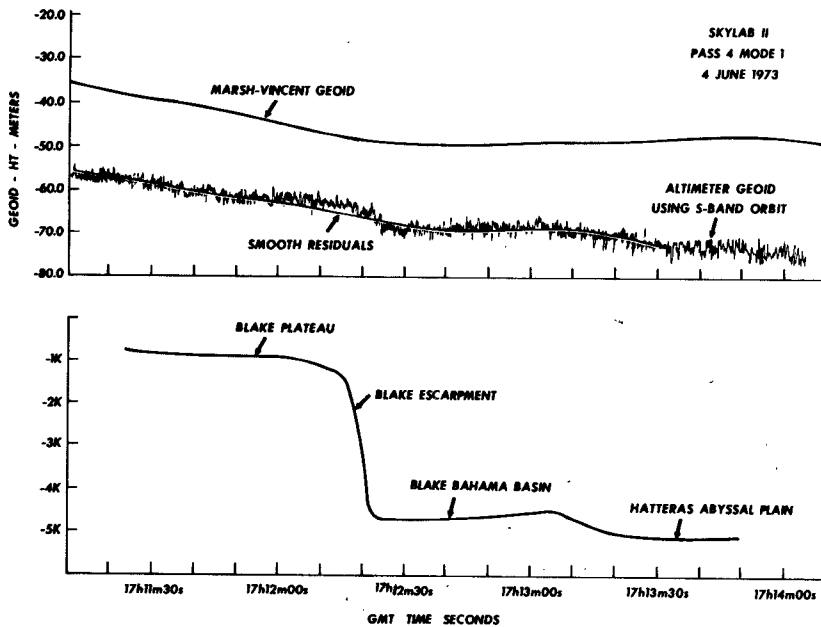


Fig. 10.

the altimeter would contribute to the improved mapping of these features.

#### Geological Structure

The underwater topography does not always correlate with the altimeter-measured ocean topography. In fact, since the equipotential gravity field is being measured, the subsurface structure can cause the surface topography to vary significantly from the subsurface topography. This effect has been seen off the east coast of the United States and in the Gulf of Mexico.

These areas and similar ones can be geologically important for plate tectonics and geological age studies. In areas where the structure is unknown, the altimeter data can be used to test an inferred structure model. A sample case is illustrated with the sea mount in Fig. 11. The altimeter data shown were obtained over the Cape Verde Islands.

Fig. 12 shows a typical model of the sea mount and the geoid and free-air gravity anomalies predicted by that model [10]. The  $\rho_w$ ,  $\rho_c$ , and  $\rho_m$  are the assumed densities of the water, crust, and mantle used in the model. In the past these marine models have been tested against shipboard gravity measurements. It should be noted that the present model does not fully account for the total altimeter-measured geoid rise over the mount. Therefore, more adjustments should be made in the assumed densities and their distributions using the altimeter data as a constraint on the model.

#### Distribution of Wave Heights

As was discussed, the recovery of wave heights and even wave-height distributions from the leading edge of the altimeter return waveforms requires a well-known

narrow transmitted pulse. Unfortunately, the Skylab altimeter was not optimized for wave-height measurements. This instrument did not have a very narrow transmitted pulse and its height tracker noise was high enough to limit the wave-height resolution to a meter or two of significant wave height. However, the feasibility of the technique has been demonstrated with the Skylab data (see Fig. 13). The significant wave heights in the figure were obtained from National Oceanic Atmospheric Administration (NOAA) hindcast of ocean conditions.

An aircraft-mounted nanosecond (approximately 2-ns-pulsewidth) radar developed by the Naval Research Laboratory (NRL) has been utilized by NASA and NRL personnel to demonstrate the detection of wave-height changes below 35 cm [7]. The GEOS-C altimeter, having better waveform sampling, is expected to improve the satellite measurement of wave height down to an accuracy approaching 25 percent of the significant wave height. The SEASAT-A altimeter is designed to obtain wave heights with a 10-percent accuracy. This system will have the advantages of a narrower transmitted pulse (<4 ns), time-expanded waveforms for easier recovery of the leading-edge shape, and lower tracker noise (<0.5 ns).

The measurement of wave heights is important as an input to wave prediction models being developed by NOAA. The broad ocean prediction of waves primarily benefits the commercial shipping industry for hazard avoidance.

#### Current Detection

All three parameters (height, waveforms, and radar cross section) measured by radar altimeters are important for the sensing of currents. The slope of the sea surface perpendicular to the flow for south-north currents should

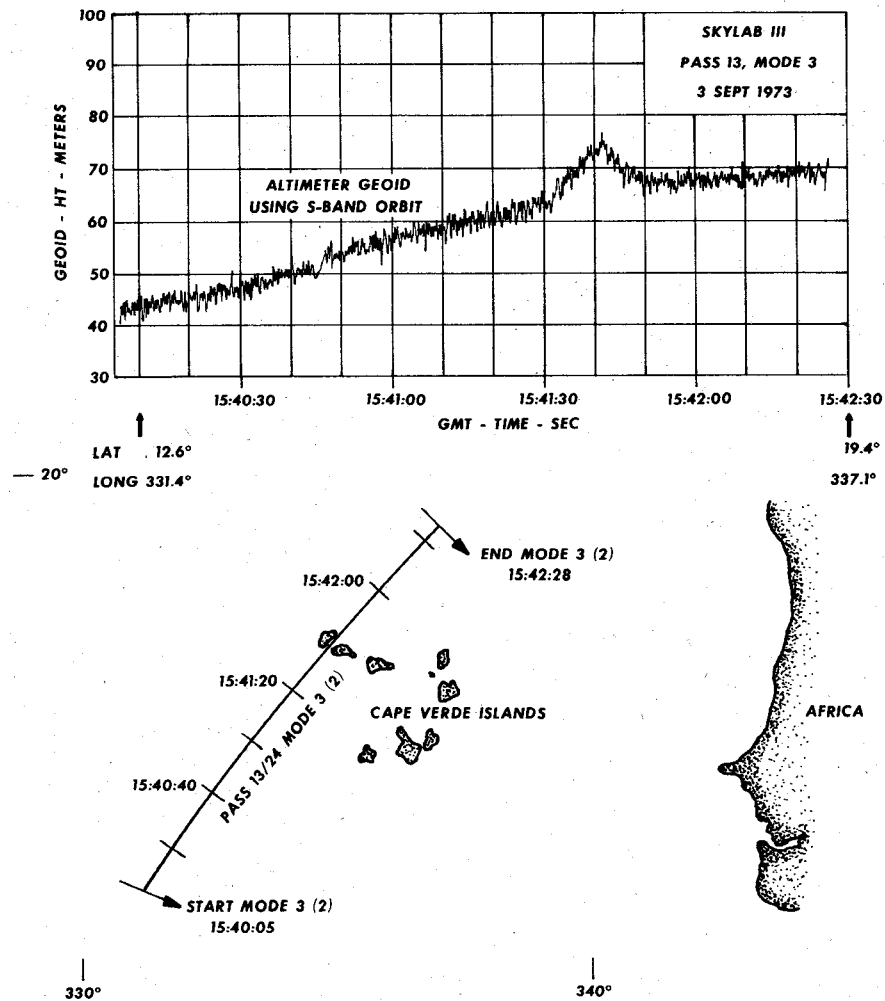


Fig. 11.

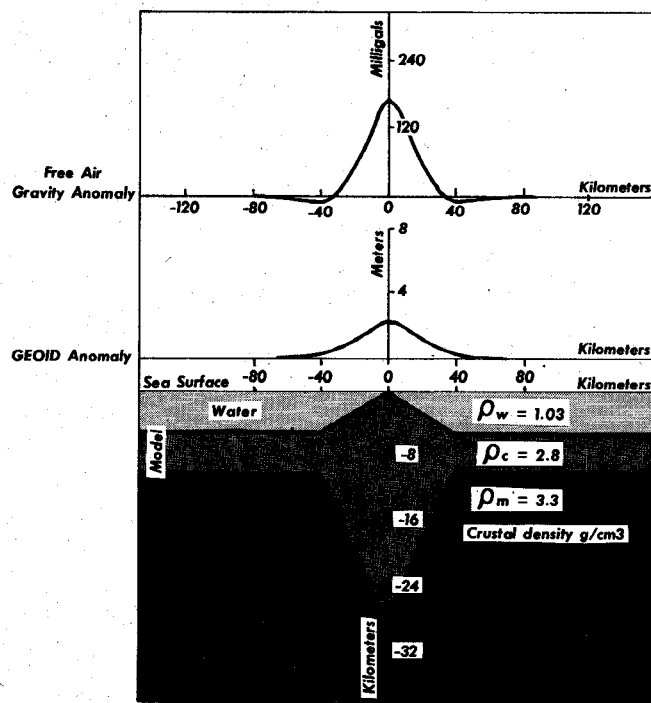


Fig. 12. Typical sea mount structural model and the corresponding gravity and geoid anomalies.

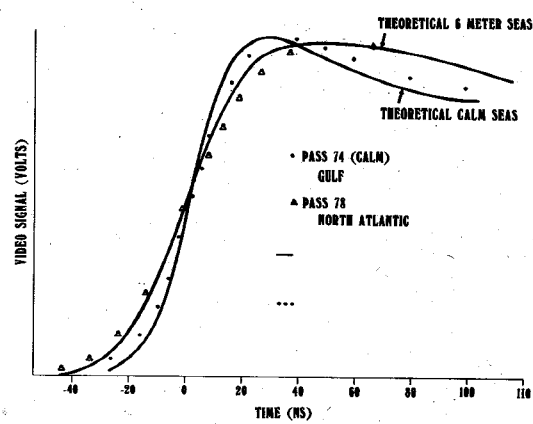


Fig. 13.

be detectable in the altitude data. The Gulf Stream, for example, has a rise of 1 m over distances of 50–100 km.

Fig. 14 shows a typical topographic feature created by the Gulf Stream or a similar current. In addition to the topographic anomaly, the current and wave interaction produces a sudden change in the wave structure. These wave structure modifications can change the radar reflectivity ( $\sigma_0$  measured with altimeter AGC) and the wave-height distributions (measured in the leading edge

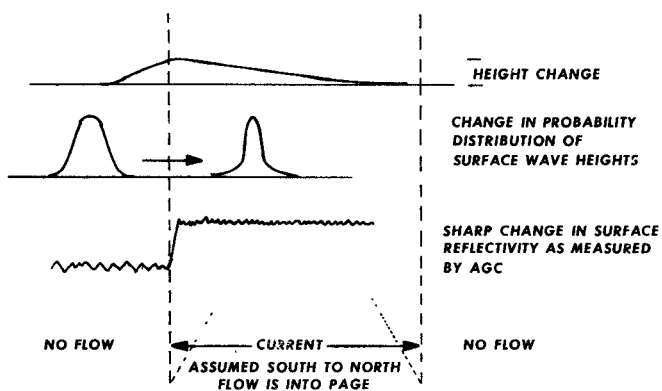


Fig. 14. Detection of ocean current with altimetry.

of the radar return waveforms). Both of these effects are also shown in the figure.

Skylab data have shown that the height changes due to currents are hard to distinguish from high-frequency geoid undulations. This is particularly true in areas where the geoid is not already well known. If altitude observations could be made during a period of time in which the current would meander, then it is possible that the geoid anomalies could be recognized and removed. However, a more direct solution to this problem might be obtained by analyzing the correlation of altitude, AGC, and waveform anomalies. The Skylab altimeter AGC consistently showed sharp changes (mostly increases) in signal strength in the vicinity of currents.

The all-weather detection and mapping of currents as possibly available from altimetry could have several important applications. The accurate positioning of the currents is important for weather modeling and ship routing. It is quite possible that the altimeter might be responding more to the mass transport of the currents than the thermal boundary normally detected by infrared scanners. If this is true, these two instrumentation systems could be complementary for the study and monitoring of current systems.

#### Land Topography

The mapping of land topography has on some occasions been extremely good. For example, in Fig. 15, an overland pass over the eastern shore of Maryland and Virginia,

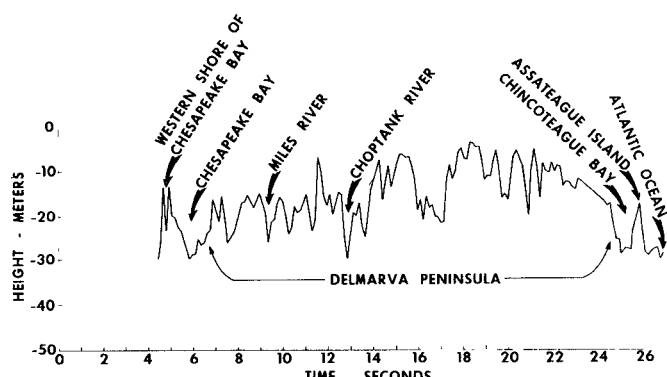


Fig. 15.

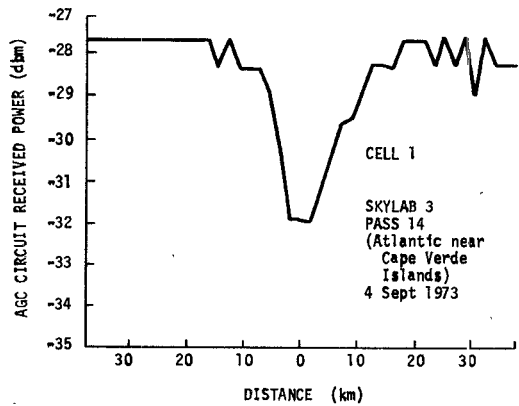


Fig. 16.

the altimeter appeared to follow the topography extremely well. This particular pass over areas with heavy vegetation, which together with the 4-nmi footprint, makes the analysis very difficult. However, the potential for mapping these areas can be visualized, and applications to forestry surveys and even snow accumulation can be predicted for the future. It should be noted that water bodies intermixed with the land serve as good height reference points for the data analysis.

#### Rain mapping

The radar backscattering cross section  $\sigma_0$  of the ocean surface is of very dependable quantity. In fact, over a wide range of sea states and wind conditions the  $\sigma_0$  measured by the Skylab altimeter has been approximately 15 dB and has not changed more than  $\pm 3$  dB. In addition, sea-state and wind changes seldom cause abrupt changes. Therefore, the ocean backscatter is consistent enough to provide a reference background for detecting rain cells.

The boundary of a rain cell is usually sharply defined and hence causes a sharp change in the altimeter AGC (see Fig. 16) [11]. The attenuation of the altimeter signal by the rain will increase with rain rate. It is easily conceivable that future altimeters can be used to spot rain cells and establish their rain rates. However, it cannot be assumed that all drops in reflectivity are due to rain or that rain will always cause a sudden drop. Therefore, if the sudden drop in AGC is suspected to be due to a change in waves, the leading edge of the returns can be analyzed to confirm a new distribution of wave heights. Similarly, if wind is suspected to cause reflectivity changes, scatterometry [12] (planned for SEASAT-A) can be used for confirming the presence of wind.

#### CONCLUSIONS

Satellite altimetry offers the physical scientists an important new source of measurements. These measurements are sufficiently unique to provide all-weather, independent observations of global topographic features. The combination of the altitude, AGC, and waveform data, together with data from other remote sensing instruments, can contribute to the accurate mapping of underwater features, detection of ocean currents, modeling of geological structure, measurement of distribution of wave heights,

rain, and rain-rate mapping, and surveying of forest heights.

In addition it has been demonstrated that altimeter data can supply precise satellite pointing information and surface reflectivity data. This information is valuable for calibrating the altimeter, and other satellite radars as well as for the design of future radar systems.

#### ACKNOWLEDGMENT

The author wishes to thank The NASA Wallops Island personnel involved in altimetry for contribution of some of the techniques and data presented in this paper. Particularly, C. Leitao, H. R. Stanley, W. F. Townsend, Dr. E. J. Walsh, C. L. Parsons, and Dr. F. E. Hoge have made substantial contributions. Also, Dr. J. D. Oberholtzer has contributed the plot of the pass over the eastern shore of Maryland and Virginia.

Dr. L. S. Miller, G. S. Hayne, and Dr. G. S. Brown of Applied Sciences Associates, Apex, N. C., have developed techniques for recovering wave height and satellite pointing and have produced some of the S-193 Skylab data results utilized in this paper.

Dr. W. T. Wells of Wolf Research and Development Corporation, Riverdale, Md., has supplied some of the methods used for geoid recovery.

E. Hofmeister and T. Godbey of General Electric, Utica, N. Y., have supplied various instrument data from which typical altimeter performance and errors were extracted.

B. Yapple, D. Hammond, and A. Shapiro of the Naval

Research Laboratory have provided technical assistance for all the present satellite altimeters and are the designers of the nanosecond radar utilized for aircraft studies.

#### REFERENCES

- [1] W. M. Kaula, "The terrestrial environment: Solid earth and ocean physics," NASA Rep. Study at Williamstown, Mass., NASA CR-1579, Aug. 1969.
- [2] R. P. Dooley, F. E. Nathanson, and L. W. Brooks, "Study of radar pulse compression for high resolution satellite altimetry," NASA CR-137474, Dec. 1974.
- [3] E. L. Hofmeister, "Analysis and measurements of the performance of a signal tracking loop for a satellite radar altimeter when excited by a random process," Ph.D. dissertation, Syracuse Univ., Syracuse, N. Y., 1973.
- [4] J. T. McGoogan, "Precision satellite altimetry," 1974 IEEE INTERCON Technical Papers, Mar. 26-29, 1974.
- [5] J. T. McGoogan, L. S. Miller, G. S. Brown, and G. S. Hayne, "The S-193 radar altimeter experiment," *Proc. IEEE (Special Issue on Modern Radar Technology and Applications)*, vol. 62, pp. 793-803, June 1974.
- [6] J. T. McGoogan, C. D. Leitao, and W. T. Wells, "Summary of skylab S-193 altimeter altitude results," NASA TMX-69355, Mar. 1975.
- [7] E. J. Walsh, "Analysis of experimental NRL radar altimeter data," *Radio Sci.*, vol. 9, pp. 711-722, Aug.-Sept. 1974.
- [8] C. C. Goad and C. F. Martin, "Effects of tropospheric and ionospheric refraction errors in the utilization of GEOS-C altimeter data," Planetary Sciences Dep., Rep. 008-74, prepared for NASA Contract NAS6-2173, Oct. 1974.
- [9] S. Vincent and J. G. Marsh, "Global detailed gravimetric geoid," NASA Goddard Space Flight Center, Rep. X-592-73-266, Sept. 1973.
- [10] C. Bowin, "Catalogue of geoidal variations for simple sea floor topographic features," Tech. Rep., NASA Contract NAS6-2585.
- [11] C. L. Parsons, "Cloud physics measurements by satellite altimeter," to be published in *J. Appl. Meteorol.*
- [12] C. T. Swift and W. F. Jones, Jr., "Satellite radar scatterometry," 1974 IEEE INTERCON Technical Papers, Mar. 1974.

## Using an Arbitrary Six-Port Junction to Measure Complex Voltage Ratios

CLETUS A. HOER, MEMBER, IEEE, AND KEITH C. ROE, MEMBER, IEEE

**Abstract**—An arbitrary six-port junction is analyzed as a microwave vector voltmeter, measuring the amplitudes and phase differences of two input signals in terms of power readings taken at the remaining four ports. The junction may be calibrated for measuring the complex ratio of these two signals using a self-calibration procedure which requires no attenuation or phase standards.

Manuscript received April 14, 1975. This work was partially supported by the Naval Sea Systems Command, USAFSAM, and the Army Metrology and Calibration Center. This is a contribution of the National Bureau of Standards not subject to copyright.

The authors are with the National Bureau of Standards, Boulder, Colo. 80302.

#### INTRODUCTION

PERHAPS the greatest impact in the field of UHF and microwave measurement in recent years has been the introduction of the automatic network analyzer (ANA). In contrast with the prior art where the key to improved accuracy was usually an improved hardware item, the procedure now is to measure the hardware imperfections and adjust the measurement results in such a way as to account for them. The key to this correction process is in the measurement of the phase as well as